TECHNISCHE MECHANIK, 30, 4, (2010), 316 – 323
submitted: October 14, 2009

Computational modeling of gradient hardening in polycrystals

S. Bargmann, M. Ekh, B. Svendsen, K. Runesson

A gradient hardening crystal plasticity model for polycrystals is introduced in Ekh et al. (2007). It is formulated in a thermodynamically consistent fashion and is capable of modeling a grain-size-dependent stress-strain response. In this contribution we extend that model to also include cross-hardening.
A free energy is stated which includes contributions from the gradient of hardening along each slip direction. This leads to hardening stresses depending on the second derivative of the plastic slip. The governing equations for a nonlinear coupled system of equations is solved numerically with the help of a dual-mixed finite element method. The numerical results show that the macroscopic strength increases with decreasing grain size as a result of gradient hardening: Moreover, cross-hardening further enhances the strengthening gradient effect.

1 Introduction

Modeling and simulation of material behavior have been an important part of engineering research during the last decades. The development of innovative engineering materials (such as light construction materials, for examples) as well as the development of classical materials (e.g. metals) requires deep knowledge on this issue. The material behavior depends on various phenomena on different scales in polycrystals. The underlying microstructure of the grains plays an important role. An important aspect is the dependence on the grain size of the macroscopic material response arising from the interaction between slips and grain boundaries. In contrast to conventional crystal plasticity, gradient theories take this aspect into account. They belong to the theories that include the micro-effects in the macroscopic modeling by assuming a complete scale separation.

Typically, the grain modeling is based on crystal plasticity with different slip directions and slip planes in each grain. In addition, strain gradients are induced in each grain. Thereby, grain boundaries will act as barriers to plastic deformation (i.e. the plastic slip). Different approaches have been formulated. A simple but effective (in the sense that it shows realistic simulation results) model is presented in Ekh et al. (2007). The model is formulated within the framework of continuum thermodynamics and finite strains. Another model by Evers et al. (2004) is motivated from physical dislocation densities and evolution equations for these, however, without any thermodynamical considerations. One disadvantage of the approach of Ekh et al. (2007) is that it does not include cross-hardening. However, this can be added in a straight-forward way, as shown in this contribution.

Cross-hardening refers to the effect that during plastic deformation in one slip system, the hardening of other slip systems are activated. This activation of multiple slip has two primary influences on the evolution of the latent hardening ratios. Firstly, regardless of the form of the self-hardening moduli, the effective latent hardening decreases with an increase in the slip system activity. It is defined by the number and intensity of active secondary systems. Secondly, multiple slip can lead to a rapid increase in the rate of hardening as compared to single slip.

The paper is organized as follows: We begin with a short reiteration of the key ideas in the modeling of gradient crystal plasticity. Subsequently, we formulate an extended version of the model presented in Ekh et al. (2007) which includes cross-hardening. The numerical implementation is carried out with the help of a dual-mixed finite element method. Hereby, the displacements and the plastic slips projected on the slip directions are the degrees of freedom. The resulting system of equations is highly nonlinear and strongly coupled. In particular, an algorithm suitable for parallelization is introduced, where each grain is treated independently as a subproblem. The macroscopic deformation gradient is imposed on the representative volume element (RVE) by solving the mechanical governing equation on the whole RVE with Dirichlet boundary conditions. For the grain boundary conditions, microclamped boundaries are assumed. Whereas the assumption for the deformation gradient represents an approach with very few constraints and, thus, a very high level of physical realism, the microclamped grain boundary condition is rather restrictive. However, grain boundary conditions represent a topic of their own and is investigated in

a different contribution, see e.g. Ekh et al. (2009). Here, we concentrate on the influence of cross-hardening in the model by (Ekh et al., 2007).

The modeling approach and the discretization are discussed by means of representative two-dimensional example. The paper ends with a discussion of the presented approach (Section 5).

2 Mathematical model

For simplicity, attention is restricted here to isothermal processes. As stated in the introduction, the model is thermodynamically based. Moreover, we postulate the existence of a potential: the volume-specific free energy density ψ. Following Ekh et al. (2007), it can be decomposed additively into an elastic and a hardening contribution, i.e. ψ_{e} and ψ_{h} respectively,

$$\psi(\boldsymbol{F}, \boldsymbol{F}_{\mathrm{P}}, \boldsymbol{\gamma}, \nabla_{\mathrm{r}}\boldsymbol{\gamma}) = \psi_{\mathrm{e}}(\boldsymbol{E}_{\mathrm{E}}(\boldsymbol{F}, \boldsymbol{F}_{\mathrm{P}})) + \psi_{\mathrm{h}}(\boldsymbol{\gamma}, \nabla_{\mathrm{r}}\boldsymbol{\gamma}) \,. \tag{1}$$

In particular, in order to include cross-hardening effects, it reads

$$\psi(\boldsymbol{F}, \boldsymbol{F}_{\mathrm{P}}, \boldsymbol{\gamma}, \boldsymbol{\nabla}_{\mathrm{r}}\boldsymbol{\gamma}) = \underbrace{\frac{\lambda}{2}\left[\mathrm{tr}\boldsymbol{E}_{\mathrm{E}}\right]^2 + \mu \boldsymbol{E}_{\mathrm{E}} : \boldsymbol{E}_{\mathrm{E}}}_{:=\psi_{\mathrm{e}}} + \underbrace{\frac{1}{2}\sum_{\alpha,\beta} H^{\mathrm{l}}_{\alpha\beta}\gamma_\alpha\gamma_\beta + \frac{1}{2}\sum_{\alpha,\beta} l_\alpha H^{g}_{\alpha\beta} l_\beta \left[\boldsymbol{\nabla}_{\mathrm{r}}\gamma_\alpha \cdot \boldsymbol{s}_\alpha\right]\left[\boldsymbol{\nabla}_{\mathrm{r}}\gamma_\beta \cdot \boldsymbol{s}_\beta\right]}_{:=\psi_{\mathrm{h}}} . \tag{2}$$

Here, λ and μ are the Lame parameters and the tensor product ":" denotes a double contraction, e.g., $\boldsymbol{A} : \boldsymbol{B} = A_{ij}B_{ij}$ for two tensors $\boldsymbol{A}$, $\boldsymbol{B}$. Furthermore, $H^{\mathrm{l}}_{\alpha\beta}$ denotes the local hardening modulus and l_α and l_β are internal length scales. Moreover, the counterpart for the gradient contribution, i.e. $\boldsymbol{H}^g$, accounts for cross-hardening effects as well:

$$H^{g}_{\alpha\beta} := [\boldsymbol{s}_\alpha \cdot \boldsymbol{s}_\beta] h_{\alpha\beta} H^{g}_{0}, \tag{3}$$

with H^{g}_{0} being a material constant, the gradient hardening modulus. Note that $H^{g}_{0} \neq H^{l}_{0}$, i.e. the gradient hardening matrix is not related to the usual interaction matrix for classical hardening. $h_{\alpha\beta}$ are coefficients of the matrix $\boldsymbol{H}^g$ - the diagonal terms are related to self-hardening of the slip systems α, whereas the off-diagonal elements induce latent hardening between the slip systems α and β. This choice is motivated by the idea that the amount of cross-hardening is influenced by the angle between the two slip systems α and β. Here, the angle between the two slip systems refers to the smaller of the two angles which exist between the slip directions $\boldsymbol{s}_\alpha$ and $\boldsymbol{s}_\beta$. For a maximum alignment of two slip directions, i.e. if $\boldsymbol{s}_\alpha \approx \boldsymbol{s}_\beta$, the influence on the newly activated slip system is rather large since $\boldsymbol{s}_\alpha \cdot \boldsymbol{s}_\beta = 1$. In case of orthogonal slip directions, the other slip system is not activated: $\boldsymbol{s}_\alpha \perp \boldsymbol{s}_\beta \Rightarrow \boldsymbol{s}_\alpha \cdot \boldsymbol{s}_\beta = 0$. $\boldsymbol{s}_\alpha$ and $\boldsymbol{s}_\beta$ are the slip direction of the active and of the newly activated slip system β, respectively.

Clearly, the volume-specific free energy density ψ is convex in all arguments, i.e. the elastic Green strain $\boldsymbol{E}_{\mathrm{E}}$, the slip $\boldsymbol{\gamma}$ and the slip gradient $\boldsymbol{\nabla}_{\mathrm{r}}\boldsymbol{\gamma}$, respectively. The elastic part of the free energy density ψ_{e} depends on the elastic Green strain $\boldsymbol{E}_{\mathrm{E}}$

$$\boldsymbol{E}_{\mathrm{E}} := \frac{1}{2}\left[\boldsymbol{C}_{\mathrm{E}} - \boldsymbol{I}\right] \tag{4}$$

with

$$\boldsymbol{C}_{\mathrm{E}} := \boldsymbol{F}_{\mathrm{E}}^{\mathrm{T}} \cdot \boldsymbol{F}_{\mathrm{E}} \tag{5}$$

being the elastic right Cauchy–Green deformation tensor. The local elastic deformation $\boldsymbol{F}_{\mathrm{E}}$ and the rate of the inelastic plastic deformation $\boldsymbol{F}_{\mathrm{P}}$ are represented by

$$\boldsymbol{F}_{\mathrm{E}} := \boldsymbol{F} \cdot \boldsymbol{F}_{\mathrm{P}}^{-1} \qquad \text{and} \qquad \dot{\boldsymbol{F}}_{\mathrm{P}} = \sum_{\alpha} \dot{\gamma}_\alpha \, \boldsymbol{s}_\alpha \otimes \boldsymbol{F}_{\mathrm{P}}^{\mathrm{T}} \cdot \boldsymbol{n}_\alpha, \tag{6}$$

as usual. Further, $\boldsymbol{\gamma} := (\gamma_1, \ldots, \gamma_{\mathfrak{g}})$ represent the amount of shear deformation in the slip-systems. In the context of crystal plasticity, the model formulation is based on the slip-system geometry as described by two unit vectors, i.e. the slip direction $\boldsymbol{s}_\alpha$ and slip-plane normal $\boldsymbol{n}_\alpha$. It is well known that often two or more crystallographically equivalent systems contribute to the plastic deformation. Therefore, $\mathfrak{a} \leqslant \mathfrak{g}$ represent the number of active glide systems. A glide system is referred to as being passive or latent if $\dot{\gamma}_\alpha = 0$, and active if $\dot{\gamma}_\alpha \neq 0$.

Since we neglect in this work the effects of any processes involving a change in or evolution of either the glide direction $\boldsymbol{s}_\alpha$ or the glide-system orientation $\boldsymbol{n}_\alpha$ (e.g., texture development), these referential unit vectors are assumed constant with respect to the reference placement. A quite common idea is to consider both $\boldsymbol{s}_\alpha$ and $-\boldsymbol{s}_\alpha$

as glide directions which will be pursued in this contribution as well (see also Ortiz and Repetto (1999)). Consequently, $\gamma_\alpha \geqslant 0$ can then be interpreted as the accumulated slip-system shear, in which case it is always positive and monotonically increasing, i.e., $\dot{\gamma}_\alpha \geqslant 0$ for all slip systems $\alpha = 1, \ldots, \mathfrak{g}$.

The hardening contribution to the free energy can be decomposed further into contributions from local and gradient hardening, respectively. By including a dependence on the slip gradient $\boldsymbol{\nabla}_{\mathrm{r}}\gamma_\alpha$, microscopic material lengthscale-dependence is introduced. The corresponding hardening moduli, $H^l_{\alpha\beta}$ and $H^g_{\alpha\beta}$, are chosen as constant and positive semi-definite measures associated with each slip-system α, β. By choosing[1] $\psi_{\mathrm{h}} = \frac{1}{2}\sum_{\alpha,\beta} H^{\mathrm{l}}_{\alpha\beta}\gamma^2_\alpha + \frac{1}{2}\sum_{\alpha,\beta} l_\alpha H^g_{\alpha\beta} l_\beta \left[\boldsymbol{\nabla}_{\mathrm{r}}\gamma_\alpha \cdot \boldsymbol{s}_\alpha\right]\left[\boldsymbol{\nabla}_{\mathrm{r}}\gamma_\beta \cdot \boldsymbol{s}_\beta\right]$, we induce crystallographic hardening and account for cross hardening via the local hardening contribution as well as the gradient hardening term.

This leads to the following dissipative hardening stresses κ_α, which are defined in such a way that they can be derived from the free energy ψ via

$$\begin{aligned} \kappa_\alpha &:= \frac{\partial\psi}{\partial\gamma_\alpha} - \mathrm{Div}\left(\frac{\partial\psi}{\partial(\boldsymbol{\nabla}_{\mathrm{r}}\gamma_\alpha)}\right) \quad \text{in } \mathcal{B}_{0,\,\text{grain}},\ \alpha = 1, 2, ..., n_{\text{slip}} \\ \kappa^{(b)}_\alpha &:= \boldsymbol{N} \cdot \frac{\partial\psi}{\partial(\boldsymbol{\nabla}_{\mathrm{r}}\gamma_\alpha)} \quad \text{on } \partial\mathcal{B}_{0,\,\text{grain}},\ \alpha = 1, 2, ..., n_{\text{slip}} \end{aligned} \tag{7}$$

see Ekh et al. (2007) for the derivation and further details. Here, $\boldsymbol{N}$ is the outward unit normal to the grain boundary $\partial\mathcal{B}_{0,\,\text{grain}}$ and the superscript "b" denotes "boundary". The hardening stresses κ_α are composed of local as well as gradient contributions, whereas the gradient tractions $\kappa^{(b)}_\alpha$ on the grain boundary $\partial\mathcal{B}_{0,\,\text{grain}}$ represent the gradient effect only. In particular, for the free energy function stated in Eq. $(2)_1$, this leads to

$$\begin{aligned} \kappa_\alpha &= \sum_\beta H^l_{\alpha\beta}\gamma_\beta - \mathrm{Div}(l_\alpha \sum_\beta H^g_{\alpha\beta} l_\beta \left[\boldsymbol{\nabla}_{\mathrm{r}}\gamma_\beta \cdot \boldsymbol{s}_\beta\right]\boldsymbol{s}_\alpha) \\ &= \sum_\beta H^l_{\alpha\beta}\gamma_\beta - l_\alpha \sum_\beta H^g_{\alpha\beta} l_\beta \left[\boldsymbol{s}_\alpha \otimes \boldsymbol{s}_\beta\right] : \left[\boldsymbol{\nabla}_{\mathrm{r}} \otimes \boldsymbol{\nabla}_{\mathrm{r}}\right]\gamma_\beta, \end{aligned} \tag{8}$$

$$\kappa^{(\mathrm{b})}_\alpha = \boldsymbol{N} \cdot \left[\sum_\beta l_\alpha H^g_{\alpha\beta} l_\beta \left[\boldsymbol{\nabla}_{\mathrm{r}}\gamma_\beta \cdot \boldsymbol{s}_\beta\right]\boldsymbol{s}_\alpha\right]. \tag{9}$$

Clearly, the extension of a regular local hardening is represented by the additional term $l_\alpha \sum_\beta H^g_{\alpha\beta} l_\beta \left[\boldsymbol{s}_\alpha \otimes \boldsymbol{s}_\beta\right] : \left[\boldsymbol{\nabla}_{\mathrm{r}} \otimes \boldsymbol{\nabla}_{\mathrm{r}}\right]\gamma_\beta$. This gradient term leads to grain size dependent hardening - although the grain size does not enter this term directly. The dissipative hardening stresses κ_α and $\kappa^{(\mathrm{b})}_\alpha$ exist within each grain and on each grain boundary, respectively.

Having introduced the basic underlying modeling ideas, we now turn to the governing equations. The mechanical problem is governed by the quasi-static balance of linear momentum

$$\boldsymbol{0} = \mathrm{Div}\boldsymbol{P} + \rho_0 \boldsymbol{b}. \tag{10}$$

The first Piola–Kirchhoff stress tensor $\boldsymbol{P}$ is derived from the free energy as usual, i.e. $\boldsymbol{P} = \partial\psi/\partial\boldsymbol{F}$. Furthermore, $\boldsymbol{b}$ represents the volume force.

The grain problem is governed by the flow rule which relates the plastic slip γ_α to the stresses. We assume a (rate-dependent) viscoplastic flow rule of the type

$$\dot{\gamma}_\alpha = \frac{1}{t_*}\,\eta_\alpha(\Phi_\alpha)\,. \tag{11}$$

Here, $t_* > 0$ is the relaxation time and $\eta_\alpha(\Phi_\alpha)$ are the overstress-functions of the Perzyna type (cf. Perzyna (1971)). The latter are chosen as non-negative and monotonically increasing for all slip systems α. In particular, a

[1] Ekh et al. (2007) chose $\psi_{\mathrm{h}} = \frac{1}{2}\sum_\alpha H^{\mathrm{l}}_\alpha\gamma^2_\alpha + \frac{1}{2}\sum_\alpha l^2_\alpha H^g_\alpha \left[\boldsymbol{\nabla}_{\mathrm{r}}\gamma_\alpha \cdot \boldsymbol{s}_\alpha\right]\left[\boldsymbol{\nabla}_{\mathrm{r}}\gamma_\alpha \cdot \boldsymbol{s}_\alpha\right]$ which accounts for crystallographic but not for cross-hardening. The later is a non-physical simplification. The same assumption is made by Vrech and Etse (2007) in case of a small deformation theory.

power law is chosen

$$\eta_\alpha(\Phi_\alpha) = \left[\frac{< \Phi_\alpha >}{C_0}\right]^m \qquad \text{with } < \Phi_\alpha >:= \frac{1}{2}\left[\Phi_\alpha + |\Phi_\alpha|\right]. \tag{12}$$

In this model, C_0 and m are constant material parameters which are the same for all slip systems α. The special case of rate-independent plasticity is retrieved in the limit when $t_*[C_0]^m \to 0$. Following Ekh et al. (2007), the quasi-static yield functions Φ_α are defined as

$$\Phi_\alpha = \tau_\alpha - [Y_\alpha + \kappa_\alpha], \tag{13}$$

where τ_α represents the resolved shear stress. Hence, the current slip resistance on each slip system α is given by $Y_\alpha + \kappa_\alpha$. Y_α is the initial yield stress and the dissipative hardening stresses κ_α are of the drag-stress type. Fully elastic behavior is characterized by $\Phi_\alpha < 0$. Consequently, then $\dot{\gamma}_\alpha = 0$. Summarizing, these considerations lead to the following viscoplastic flow rule

$$\dot{\gamma}_\alpha = \frac{1}{t_*}\left[\frac{< \tau_\alpha - [Y_\alpha + \kappa_\alpha] >}{C_0}\right]^m. \tag{14}$$

3 Numerical approximation

Since this system cannot be integrated analytically, this section briefly summarizes the formulation of the numerical approximation scheme we used. For more details and a comparison about different mechanical boundary condition assumptions, the reader is referred to Ekh et al. (2007). For the temporal discretization, a backward (implicit) Euler integration for the evolution equations is applied. The state at $t = t_{n-1}$ is assumed to be known for a given time history of the pertinent loading. For example, this leads to the incremental, semi-discretized version of the equation for the rate of the inelastic deformation (i.e. given in Eq. $(6)_2$)

$$\boldsymbol{I} - \boldsymbol{F}_{\mathrm{P}\,n-1} \cdot \boldsymbol{f}_{\mathrm{P}\,n} - \Delta t \sum_\alpha \frac{\gamma_{\alpha\,n} - \gamma_{\alpha\,n-1}}{\Delta t}\left[\boldsymbol{s}_\alpha \otimes \boldsymbol{n}_\alpha\right] = \boldsymbol{0}, \tag{15}$$

with $\Delta t = t_n - t_{n-1}$ denoting the current time step. The inverse of the plastic part of the deformation gradient is initialized as $\boldsymbol{f}_{\mathrm{P}\,0} = \boldsymbol{I}$. Furthermore, we assume that no plastic slip exists in the beginning of the deformation process, i.e. $\gamma_\alpha(t = 0) = 0$.

The spatial discretization is done with a dual-mixed finite element algorithm, whereby the primary unknowns are the displacement $\boldsymbol{u}$ and the artificial scalar g_α

$$g_\alpha := \boldsymbol{\nabla}_{\mathrm{r}}\boldsymbol{\gamma}_\alpha \cdot \boldsymbol{s}_\alpha. \tag{16}$$

g_α can be interpreted as the directional gradient of the slip γ_α along the slip direction $\boldsymbol{s}_\alpha$. Thereby, the plastic slip γ_α and the scalar g_α are approximated independently in the reference configuration $\mathcal{B}_0$ of the material in question and the gradient equation

$$g_\alpha - \boldsymbol{\nabla}_{\mathrm{r}}\boldsymbol{\gamma}_\alpha \cdot \boldsymbol{s}_\alpha = \boldsymbol{0} \tag{17}$$

is a global equation in space. Such an approach is denoted the dual mixed space-variational formulation, see Ekh et al. (2007) for further details. Via such a format, it is possible to choose the finite element approximation of the scalar g_α one order higher than the finite element approximation of the plastic slip γ_α. The slip γ_α is solved for iteratively on the element level.

In total, this leads to a three-level iteration scheme. First, in an outer iteration loop called “grain boundary iteration loop” we solve for the displacements $\boldsymbol{u}$ on the grain boundaries. Then, in the “inner grain iteration loop”, updated values of displacements $\boldsymbol{u}$ and the scalars g_α within each grain are computed. During the “inner grain iteration loop”, the displacements on the grain boundaries are kept fixed, given the updated values from the “grain boundary iteration loop”. Therefore, the resulting algorithm is suitable for parallelization. In each “inner grain iteration loop”, a monolithic Newton–Raphson solution strategy is applied.
In order to be able to apply this separation, the underlying finite element mesh has to respect the grain boundaries. In addition to the two loops, a third iteration loop is carried out on the element level. The purpose of this “local iteration loop” is to find updated values for the slip γ_α in each Gauss point, given the values of the displacement $\boldsymbol{u}$ and the artificial scalar g_α (as provided from the inner grain iteration loop).

Remark:
A different numerical approximation scheme which has been applied to the original model of Ekh et al. (2007) is introduced in Bargmann et al. (2009). That scheme is also suitable for the model introduced in this contribution, i.e. including the cross-hardening effect. The formulation of an incremental variational principle describing gradient crystal plasticity in Bargmann et al. (2009) is based on the direct exploitation of the dissipation principle to derive all field relations and (sufficient) forms of the constitutive relations as based on the free energy density ψ and a dissipation potential d. Due to the variational character of the problem, the resulting iteration matrix is symmetric. Moreover, only the "grain boundary iteration loop' and the "inner grain iteration loop" are necessary - both solving for the displacements $\boldsymbol{u}$ and the plastic slip γ_α as primary unknowns. The procedure applied in Bargmann et al. (2009) is also suitable for parallelization as it is based on the same idea of grain separation. It leads to a two-level iteration scheme.

4 Simulations

To gain further insight into the effect of cross-hardening in the modeling approach being pursued here, we now look in detail at the hardening behavior of a two-dimensional inelastic polycrystal with side length L. This side length L does not enter the model formulation directly. Rather, it influences the results via the position of the global nodes which vary along with a variation of L. In order to capture the size-dependence stress-strain response, the side length L is varied during simulations. A double slip system is assumed in each grain which leads to $\mathfrak{g} = 4$, see Figure 1 (right). The RVE consists of 25 grains and is subdivided into 11392 finite elements, as depicted in Figure 1 (left). Grain boundaries are respected by the mesh. Each of the triangular elements has 3 nodes and each node has 6 degrees of freedom (two displacements and four slips). Moreover, nodes on the inner grain boundaries have been doubled in order to allow for a separate computation of the grains. During the simulations, 200 time steps have been used.

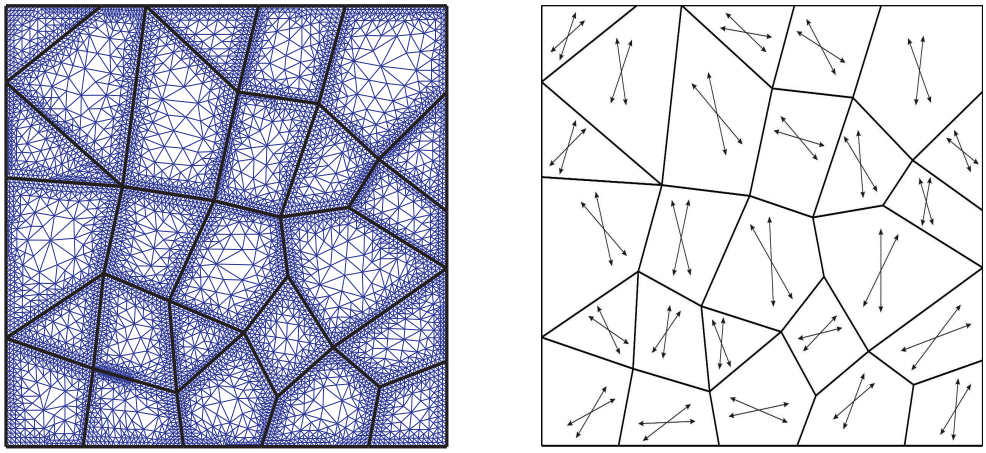

Figure 1: On the left the geometry and its discretization of the RVE is depicted. It consists of 25 grains which are approximated by triangular elements. Grain boundaries are respected by the mesh. A random two-slip system is assumed. The random slip directions are illustrated schematically on the right. The boundary conditions are explained in the text.

Plain strain is assumed and the case of simple shear on the macro-scale is studied. Consequently, the macroscopic deformation gradient reads $\boldsymbol{F} = \boldsymbol{I} + \bar{\gamma}\boldsymbol{e}_1 \otimes \boldsymbol{e}_2$, where $\bar{\gamma}$ is the macroscopic shear deformation. For the boundary conditions of the mechanical subproblem, we prescribe the displacements $\boldsymbol{u}$ at the whole RVE boundary, i.e. Dirichlet boundary conditions are prescribed on the entire boundary. The constant loading rate is set constant at $0.2\ [1/\mathrm{s}]$. Computations are carried out with $\bar{\gamma}_{\max} = 0.15$.

For the grain subproblem, we assume micro-clamped boundary conditions, i.e.

$$\gamma_\alpha = 0 \qquad \text{on } \partial\mathcal{B}_{0,\text{grain}}. \tag{18}$$

Whereas the mechanical boundary conditions are not very restrictive and physically meaningful, we are aware of the fact that the grain boundary conditions are, from a physical point of view, too restrictive because they do not allow slip interaction between the grains. Studying the influence of the latter on the results is a topic of its own

(see Ekh et al. (2009)) and not part of this contribution.

The material parameters used in the simulations are stated in Table 1.

parameter	symbol	value	
Young's modulus	E	$2 \cdot 10^5$	[MPa]
Poisson's ratio	ν	0.3	
local hardening modulus	H_0^l	500	[MPa]
gradient hardening modulus	H_0^g	$3 \cdot 10^7$	[MPa]
internal length scale	l_α	10^{-2}	[μm]
initial yield stress	Y_α	300	[MPa]
relaxation time	t_*	10^4	[s]
material constant	C_0	1	[MPa]
rate sensitivity parameter	m	1	

Table 1: Material parameters used in the simulations. Usually, the initial yield stress Y_α and the local hardening modulus H_α^l are three orders lower than the elasticity modulus E - as chosen in this particular example. The local hardening modulus H_α^l is chosen in such a way that cross-hardening effects are included: $H_{\alpha\alpha}^{\mathrm{l}} = H_0^{\mathrm{l}}$ and $H_{\alpha\beta}^{\mathrm{l}} = \frac{1}{10} H_0^{\mathrm{l}}$ for $\alpha \neq \beta$. Thus, the self-hardening contribution within the slip-system α is larger than the hardening cross-hardening contribution.

In order to systematically simulate size dependent material behavior of the polycrystal, the side length L has been varied. Moreover, simulations have been run for the model excluding and including cross-hardening. The first option is done by choosing $h_{\alpha\beta} = \delta_{\alpha\beta}$, where $\delta_{\alpha\beta}$ denotes the Kronecker symbol. In order to compute the stress-strain curves for the model including cross-hardening we set $h_{\alpha\beta} = 1$ for $\alpha = \beta$ and $h_{\alpha\beta} = 0.25$ for $\alpha \neq \beta$. Thus, the cross-hardening from one slip system to the next is less than the self-hardening on the active slip system.

First, we take a look at the stress-strain responses. In Figures 3 and 4, these are shown for $L = 5$ μm, $L = 10$ μm, $L = 20$ μm, $L = 40$ μm, and $L = 100$ μm - for both the cases without and with cross-hardening. Clearly, the influence of the grain size can be seen. The smaller the RVE, the stiffer its material response. From the modeling point of view, this feature is accomplished by including a gradient contribution into the free energy density ψ and, consequently, into the slip law. A dependence on the grain size is seen. In Figure 3, the stress-strain curves are plotted for our model excluding the effect of cross-hardening. The results including cross-hardening are plotted in Figure 4. Once more, the grain size dependent hardening behavior can clearly be identified and is in accordance to the experimental findings of Hall (1951) and Petch (1953): the smaller the grain size, the stiffer the polycrystals behave. The experiments of Hall (1951) and Petch (1953) also show a size-dependence of the yield stress. This feature is not captured by this basic model. However, enhancing this model in this direction is part of ongoing research. Moreover, for the smaller samples the cross-hardening leads to a stiffer response than in the case of self-hardening. For larger samples, the effect is negligible.

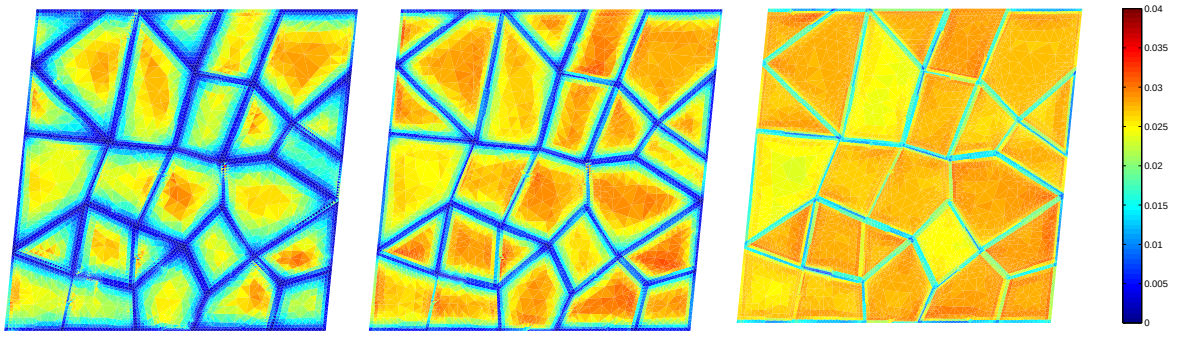

Figure 2: Including cross-hardening. The effective hardening strain $\gamma_{\mathrm{eff}} = \sqrt{\gamma_1^2 + \gamma_2^2 + \gamma_3^2 + \gamma_4^2}$ at $\bar{\gamma} = 0.05$ is depicted. From left to right the accumulated plastic strain field for grain-structure side lengths $L = 5$ μm, $L = 10$ μm, and $L = 40$ μm are depicted. The evolution of the slip-system shear γ_α is given in Eq. (14). The displacement field inside the grain-structure is unconstrained.

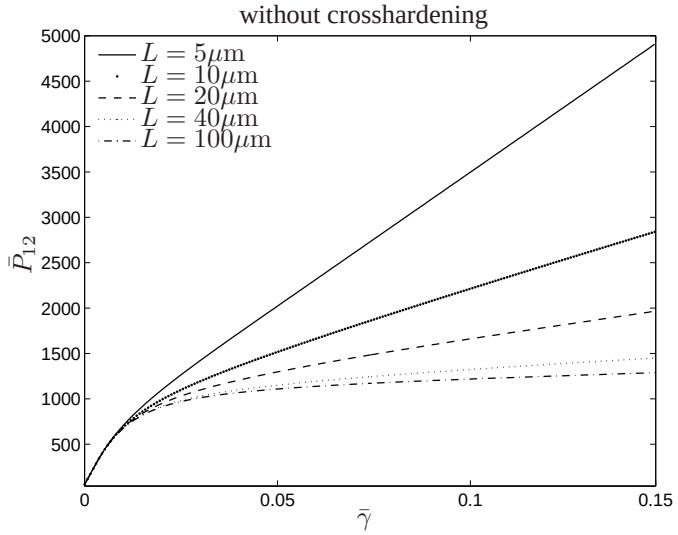

Figure 3: The macroscopic stress–strain response ($\bar{P}_{12}$ vs. $\bar{\gamma}$) showing the size dependence on the amount of hardening is depicted for RVE lengths $L = 5\ \mu$m, $L = 10\ \mu$m, $L = 20\ \mu$m, $L = 40\ \mu$m, and $L = 100\ \mu$m. The effect of cross-hardening is neglected. The larger the grain size, the softer responses the material.

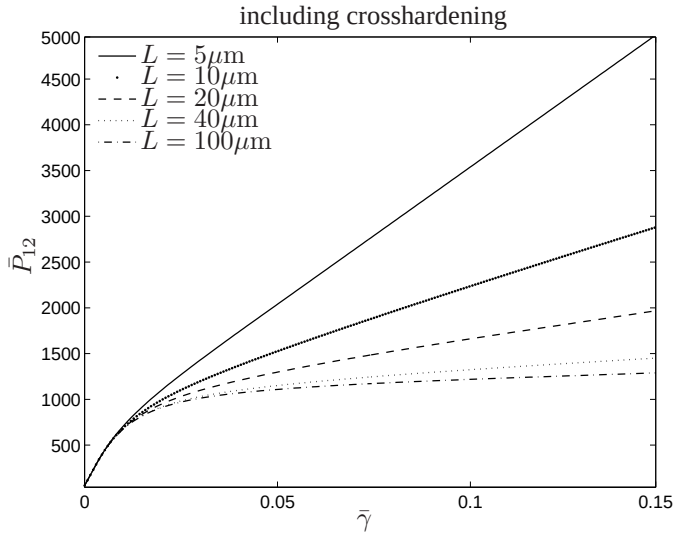

Figure 4: The macroscopic stress–strain response ($\bar{P}_{12}$ vs. $\bar{\gamma}$) showing the size dependence on the amount of hardening is depicted for RVE lengths $L = 5\ \mu$m, $L = 10\ \mu$m, $L = 20\ \mu$m, $L = 40\ \mu$m, and $L = 100\ \mu$m. During these simulations, the effect of cross-hardening is included. This leads to a stiffer material response than in the case of pure self-hardening. Again, the larger the grain size, the softer responses the material.

5 Conclusion

Motivated by the results presented in Ekh et al. (2007), we added the effect of cross-hardening into the gradient crystal plasticity model. In this approach, the volume-specific free energy was assumed to include contributions from local as well as non-local hardening. The latter was influenced by the plastic slip gradient along each slip direction. The numerical simulations showed that small grains lead to stiffer hardening responses. Unfortunately, the effect of cross-hardening is rather small in this approach. The arising coupled boundary value problem was discretized within the finite element method. We conclude that the proposed model formulation and the dual-mixed finite element algorithm are convenient for modeling size-dependent hardening including cross-hardening in polycrystals.

Acknowledgement

The authors are grateful to the anonymous referee for his/her helpful comments and suggestions. We wish to gratefully acknowledge the support of the Swedish Research Council. Part of this work was done while S.B. was a visiting PostDoc at Chalmers University of Technology whose hospitality is also gratefully acknowledged.

References

Bargmann, S.; Svendsen, B.; Ekh, M.; Runesson, K.: The algorithmic formulation of large deformation extended crystal plasticity. *submitted*.

Ekh, M.; Bargmann, S.; Grymer, M.: Influence of grain boundary conditions on modeling of size-dependence in polycrystals. *submitted*.

Ekh, M.; Grymer, M.; Runesson, K.; Svedberg, T.: Gradient crystal plasticity as part of the computational modeling of polycrystals. *International Journal for Numerical Methods in Engineering*, 72, (2007), 197–220.

Evers, L.; Brekelmanns, W.; Geers, M.: Non-local crystal plasticity model with intrinsic ssd and gnd effects. *J. Mech. Phys. Solids*, 52, (2004), 2379–2401.

Hall, E.: The deformation and ageing of mild steel: III discussion of results. *Proceedings Physical Society London B*, 64, (1951), 747–753.

Ortiz, M.; Repetto, E. A.: Non-convex energy minimization and dislocation structures in ductile single crystals. *Journal of the Mechanics and Physics of Solids*, 47, (1999), 397–462.

Perzyna, P.: Thermodynamic theory of viscoplasticity. *Advances in Applied Mechanics*, 11, (1971), 313–354.

Petch, N.: The cleavage strength of polycrystals. I. *Journal of Iron and Steel Institute*, 174, (1953), 25–28.

Vrech, S.; Etse, G.: FE approach for thermodynamically consistent gradient-dependent plasticity. *Latin American Applied Research*, 37, (2007), 127–132.

Addresses:
S. Bargmann and B. Svendsen, Institute of Mechanics, Leonhard-Euler-Str. 5, TU Dortmund, 44227 Dortmund, Germany.
M. Ekh and K. Runesson, Department of Applied Mechanics, Chair of Material and Computational Mechanics, Chalmers University of Technology, Gothenburg, Sweden
email: swantje.bargmann@tu-dortmund.de